Propagation Loss of Line-Defect Photonic Crystal Slab Waveguides

Wan Kuang
Boise State University

Woo J. Kim
University of Southern California, Los Angeles

Adam Mock
University of Southern California, Los Angeles

John O'Brien
University of Southern California, Los Angeles

Propagation Loss of Line-Defect Photonic Crystal Slab Waveguides

Wan Kuang, *Member, IEEE*, Woo Jun Kim, Adam Mock, and John O'Brien, *Senior Member, IEEE*

Abstract—**Photonic crystal slab waveguides are created by inserting a linear defect in two-dimensional (2-D) periodic dielectric structures of finite height. Photonic crystals provide 2-D in-plane bandgaps through which light cannot propagate, however, the fact that the waveguide modes must be index-confined in the vertical direction implies that the propagation loss is strongly dependent on the out-of-plane radiation loss. We present a fully three-dimensional finite-difference time-domain numerical model for calculating the out-of-plane radiation loss in photonic crystal slab waveguides. The propagation loss of the single-line defect waveguide in 2-D triangular lattice photonic crystals is calculated for suspended membranes, oxidized lower claddings, and deeply etched structures. The results show that low-loss waveguides are achievable for sufficiently suspended membranes and oxidized lower cladding structures. The roles of the photonic crystal in out-of-plane loss of the waveguide modes are further analyzed. It is predicted that the out-of-plane radiation loss can be reduced by shifting one side of the photonic crystal cladding by one-half period with respect to the other sides along the propagation direction.**

Index Terms—**Finite-difference time domain (FDTD), photonic crystals, propagation loss, waveguides.**

I. INTRODUCTION

TWO-dimensional (2-D) photonic crystal defect waveguides have been the subject of active research [1]–[3] due to their potential to be a basic building block for densely integrated optics. They are most simply formed by inserting a linear defect in a 2-D triangular lattice of air holes in a dielectric slab. Photonic crystals provide a 2-D in-plane frequency bandgap for the guided modes of the slab. In the vertical direction, light is localized to the slab by means of total internal reflection. Although the in-plane photonic bandgap prohibits light to propagate anywhere but along the linear defect, a much weaker index confinement in the vertical direction raises the concern for the out-of-plane radiation loss.

Quantitative characterization of the propagation loss is crucial in waveguide design. As with the conventional slab waveguides, even propagation modes that are confined in the core experience radiation loss due to the penetration of exponentially decaying

field in the substrate. In addition, the defect waveguide modes that lie above the light line of the claddings are likely to couple with the radiation modes. This coupling will cause the field to radiate energy out of plane. Waveguide modes that are not properly confined in the vertical direction, although still propagating along the defect due to the existence of the in-plane bandgap, will eventually radiate out of plane.

In practice, waveguide mode can also leak energy in-plane as it propagates along the defect due to an insufficient number of periods of photonic crystal cladding. The photonic bandgap is formed as a result of a periodic modulation of dielectric constant with infinite periodicity. A practical photonic crystal device has a finite number of periods that allows the light tunneling through the bandgap barrier. In general, the waveguide mode decays by a few orders of magnitude after seven periods of photonic crystals [4]. However, the rate of decay in the lateral direction is also influenced by the waveguide design and the location of the mode in the Brillouin zone. Increasing the hole radius generally leads to a better lateral confinement and therefore minimizes the energy overlaps between adjacent waveguides. Nonetheless, channel crosstalk is one of the major issues for designing a densely integrated photonic crystal circuitry.

Another major source of loss for photonic crystal defect waveguides is related to the fabrication process. Photonic crystals patterned with e-beam lithography sometimes suffer from minor dislocations. The surfaces of the sidewalls are also likely to have some degree of roughness and slant after dry etching. All these imperfections can be a source of scattering loss. Quantifying radiation loss of the modes due to fabrication imperfections is a difficult issue. As fabrication imperfections are a rather random phenomena in nature, statistical analysis is required for characterizing the dislocation and roughness. The problem itself can be classified into fabrication-induced in-plane propagation loss and vertical radiation loss. For the in-plane loss, the fabrication imperfection diminishes the photonic bandgap, allowing the field to escape the photonic crystal cladding. A few authors have attempted to address this issue in [5] and [6]. However, more importantly, the scattering of the field at imperfections cause radiation out of plane. Unlike the in-plane case, where the scattered field needs to go through several periods of photonic crystal, the out-of-plane scattering cannot be trapped and is therefore more sensitive to fabrication imperfections. As the problem is intrinsically three dimensional (3-D), it requires an efficient 3-D model to handle. Recently, Hughes *et al.* [7] formulated the problem with Green's function and took scattering as a dipole radiation.

In this paper, transmission properties of the photonic crystal defect waveguides are focused on the vertical radiation loss that is intrinsic to the structures. The in-plane loss due to insufficient

number of photonic crystal cladding periods is insignificant and thereby ignored in the analysis. The extrinsic loss due to fabrication is not considered either.

Since numerically modeling the exact 3-D waveguides is hardly realistic due to an exorbitant amount of memory and computational demand, an alternative approach is required. Earlier works [8], [9] simplified the 3-D waveguides with its 2-D cross section along the propagation direction. They essentially approximate a planar photonic crystal waveguide as a one-dimensional (1-D) array of grooves. However, lateral localization of the defect waveguide mode inevitably spreads the mode distribution in the reciprocal space. The lack of lateral confinement in the model results in a calculated out-of-plane loss more representative of 1-D gratings than for actual photonic crystal waveguides.

Conceptually similar to the models above, but improved by adding the lateral modal confinement, Lalanne *et al.* [10] proposed a frequency-domain S-matrix-like approach. A pseudo-periodic plane-wave (Fourier) basis is used for the in-plane direction, and an artificial periodization with absorbing boundaries for the vertical direction. It, therefore, results in an analysis of a 2-D transverse cross section of the photonic crystal. The model is capable of predicting the out-of-plane radiation losses of the photonic crystals achievable with holes etched into the substrate, but fails to address the out-of-plane losses of waveguides produced by the introduction of a linear row of defects because such structures are no longer fully periodic. It was further refined in [11] and [12] to include defects in the in-plane direction. It computes only the modes that are confined by photonic crystals laterally. However, the truncation of the Fourier harmonics leads to an accuracy estimated at $0.1 \, \mathrm{dB}/100 \, \mu\mathrm{m}$ [11], or 10 dB/cm, making the method incapable of predicting low-loss behavior.

Reducing the length of the waveguides so that they are capable of being directly solved, Hadley [13] calculated the out-of-plane radiation losses of defect waveguide by solving 3-D Helmholtz equations with a finite-difference technique. The method proves to be straightforward but it also raises the issue on source excitation efficiency, i.e., how many periods does it take to form a real Bloch defect waveguide mode. The energy that is not coupled to the guided defect waveguide modes tends to radiate off-plane, however, it propagates along as it dissipates. Simulations with short propagation distances are more vulnerable to slowly decaying radiation modes since their energies might be mistakenly included as output power. Because the calculation cannot distinguish the noise caused by source coupling, the method left those questions unanswered.

In this paper, a fully 3-D finite-difference time-domain (FDTD) model is presented to predict the out-of-plane losses of line-defect photonic crystal slab waveguides. In Section II, two numerical approaches, either computing the ratio of power loss to propagating power or calculating the quality factor of the waveguide modes, are introduced. Both methods are derived from the results of 3-D FDTD simulations. The propagation loss of a single-line defect waveguide in a triangular lattice photonic crystal is calculated in Section III for suspended-membrane oxidized lower claddings and deeply etched structures. The role
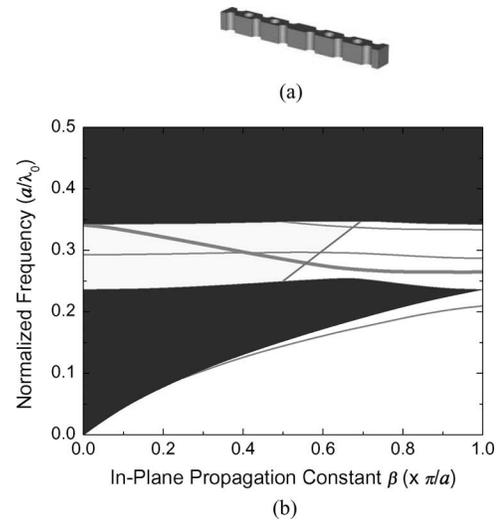
Fig. 1. (a) Structure of single-line defect waveguide for the numerical simulation. (b) Photonic band diagram of the waveguide. The *dark gray region* indicates the modes of the bulk photonic crystals and *light gray area* represents the vertical radiation light cone mapped in the propagation direction.

of the photonic crystal in forming waveguide modes is further analyzed and a type-B photonic crystal waveguide is proposed in Section IV. We will show that the out-of-plane radiation loss can be reduced by an order of magnitude by shifting the photonic crystal claddings one-half period with respect to each other along the propagation direction.

II. METHOD OF ANALYSIS

We present a fully 3-D method, which is similar to the technique used in quality factor calculation for microcavity [14]. The work presented here expands on our earlier report [15], [16]. The photonic crystal defect waveguides are modeled with a 3-D FDTD method [17], [18] using message passing interface (MPI) [19], [20] to run in a parallel environment. Discretization is no less than 20 points per inter-hole spacing. Fig. 1(a) shows the computational domain that is terminated by Berenger's perfect matched layer absorbing boundary condition (PML-ABC) [21] except in the propagation direction, where a periodic boundary condition is applied instead. An order-N [22] conformal technique is applied in handling cylinders to overcome the staircase of the original Cartesian grid FDTD formulation. The eigenmodes are given by the peaks in the frequency spectrum of the complex field components recorded at various low-symmetry locations for a given in-plane propagation constant β.

Fig. 1(b) shows the photonic band diagram of a suspended membrane photonic crystal waveguide. The dark gray region indicates the modes of the bulk photonic crystals in the propagation direction. The propagation loss of the lowest order even mode in the bandgap, which is marked with a thick curve in the dispersion diagram, will be analyzed in detail later. In the vertical direction, the propagation mode is confined by the index contrast of the dielectric membrane and the air cladding. The light gray area in Fig. 1(c) indicates the radiation light cone mapped on the propagation direction. The waveguide mode that is above the light line can couple with the continuous spectrum of the radiation modes.

To calculate the vertical radiation loss, the waveguide is excited by a single frequency dipole source whose frequency is given by the phase shift across the unit cell used in the periodic boundary condition. A traveling field is emulated by means of the double orthogonal excitation [23] in which a sinusoidal excitation is applied to the real parts of the field component and a cosinusoidal excitation is applied to the imaginary parts. The energy of the unwanted modes is suppressed by applying a time-domain band-pass filter whose central frequency aligns with the dipole source frequency. The filter is implemented as a convolution of a frequency-shifted window function and the instantaneous electromagnetic field components in the time domain. The common window functions can be found in any digital signal processing handbook [24]. A window function is a low-pass filter whose Fourier transform concentrates predominantly around $\omega = 0$. To obtain a band-pass filter, the window function is multiplied by a $\sin(\omega_0 t)$ function, which has the effect of shifting the pass band of the window from $\omega = 0$ to $\omega = \omega_0$. Here, a Blackman window of at least 30 000 time steps is employed with a side-mode suppression ratio larger than 57 dB and a bandwidth of less than 0.005 in normalized frequency.

The Poynting vectors through the top and bottom planes in the vicinity of the perfectly matched layer are summed up at every instant as vertical power flow. Those through the longitudinal plane are summed as in-plane power flow. The vertical radiation loss $\alpha_\perp$ is calculated from the ratio of the vertical power flow $P_\perp$ to the in-plane flow P_t after a steady state is achieved

$$\alpha_\perp = -\frac{\log(1 - P_\perp/P_t)}{a}. \tag{1}$$

By employing the periodic boundary condition and the filter window, this power ratio method emulated an infinitely long waveguide structure and thereby eliminates the confusion incurred by the mode excitation efficiency and surface-wave propagation in loss calculations if a finite-length waveguide is used. The numerical noise of the method is estimated to be less than 0.01 cm^{-1}, which is the out-of-plane radiation loss calculated by this method for a rigorously guided ridge waveguide.

Alternatively, waveguide loss can be obtained directly from the Fourier spectrum. The underlying principle is similar to the lifetime or the quality factor calculation in a resonant cavity. The waveguide mode in a finite structure is not lossless, the energy in the mode $U(t)$ decays as

$$U(t) = U(t_0) \exp\left(-\frac{\omega_0(t - t_0)}{Q}\right) \tag{2}$$

where the quality factor of the mode Q is given by the ratio of the mode frequency ω_0 and the full-width at half-magnitude $\Delta\omega$ of the Lorentizen energy spectrum centered at ω_0

$$U(\omega) = \frac{\Delta\omega}{(\omega - \omega_0)^2 + (\Delta\omega/2)^2}. \tag{3}$$

The quality factor is calculated from the ratio of the full-width at half-magnitude of the cavity resonance in the frequency domain $\Delta\omega$ to center frequency ω_0. The difficulty of this approach is an insufficient frequency resolution directly from the Fourier spectrum; the smallest identifiable spectral width usually cannot resolve a quality factor higher than a few hundred. Distortion
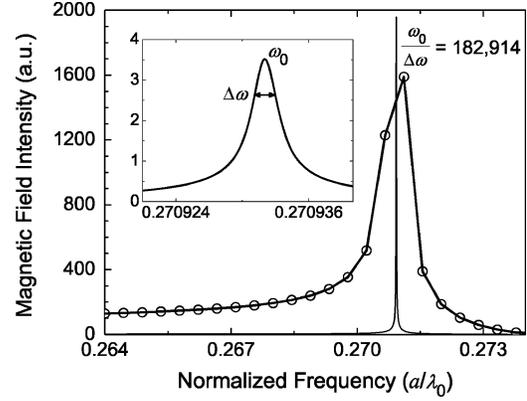
Fig. 2. Pade approximation for the lowest defect mode in W1 waveguide Fourier spectrum of a single-line defect suspended membrane photonic crystal waveguide for the propagation constant $\beta = 0.65\pi$ in the normalized frequency range of 0.264 and 0.274 as *open circles* and its Pade approximation for the interpolated frequency as a *blue curve*. The inset shows the detailed spectrum at the resonance frequency ω_0.

to the spectrum is also introduced because the numerical simulation terminates before the impulse response is fully evolved. This has the effect of viewing the true time-domain response through a rectangular window, which translates mathematically into the convolution of the true spectrum with a sinc function. The convolution widens the peaks in the spectrum among other effects. This distortion can be reduced by increasing the time response window, but at the price of a longer simulation time. Pade approximation addresses the problem by extrapolating the electromagnetic field in the time domain beyond the actual simulation window [25], [26]. The discrete Fourier transform (DFT) series is interpolated with a Pade function, which is the ratio of an order I and an order J polynomials $Q_I(\omega_k)$ and $D_J(\omega_k)$

$$P(\omega_k) = \frac{Q_I(\omega_k)}{D_J(\omega_k)} = \frac{\sum_{i=0}^{I} \alpha_i(\omega_k)^i}{\sum_{j=0}^{J} \beta_j(\omega_k)^j}. \tag{4}$$

Taking β_0 to be unity, coefficients α_i and β_j in (4) can be solved with the Fourier spectrum at ω_k. The resulting continuous Pade function has a frequency resolution significantly improved beyond the original Fourier spectrum. By combining Pade approximation with the DFT, the quality factors of all waveguide modes can be determined with just one FDTD simulation.

An important numerical issue of interpolating Fourier series with Pade's polynomials using (4) is worth noting. Both polynomials $Q_I(\omega_k)$ and $D_J(\omega_k)$ are exponential functions of frequency, the numerical errors due to the truncation of a 64-bit floating point number increase as the order of the polynomials increases. The amount of numerical error is also not uniformly distributed. Higher order terms of the polynomials suffer more significantly than do the lower order terms. It is usually advantageous to normalize the frequency ω_k so that the exponents of ω_k predominantly distribute around unity to alleviate the numerical round-off errors.

Fig. 2 shows the interpolated frequency spectrum of the magnetic field from the Pade polynomials as well as the Fourier spectrum as open circles for the first defect waveguide mode in

TABLE I
PHOTONIC CRYSTAL DEFECT SLAB WAVEGUIDES CONSIDERED IN THE CALCULATIONS

Waveguides	Suspended Membrane	Oxidized Cladding	Deeply Etched
Layer description[a] [b]	Air	Air	Air
			AlGaAs (1.0)
	$GaAs$ (0.6)	$GaAs$ (0.6)	$GaAs$ (1.0)
	Air (1.0, 3.0)	Al_xO_y (2.0, 5.0)	AlGaAs (6.0)
	$GaAs$	$GaAs$	$GaAs$

[a]A refractive index of 3.4 is assumed for $GaAs$, 3.0 for AlGaAs, 1.6 for Al_xO_y, and 1.0 for air.

[b]The normalized thickness d/a appears in parentheses after the material.

the photonic bandgap at $\beta = 0.65\pi/a$. Since the full-width at half-magnitude $\Delta\omega$ is defined in the optical power, it should be given by the full-width at $1/\sqrt{2}$ of the maximum in the figure. The waveguide mode has an extremely high quality factor as it lies outside the radiation light cone.

The quality factor Q describes the waveguide loss per unit time. The propagation loss, which is generally expressed as the loss per unit distance, can be related to the Qs of the waveguide modes by [27]

$$U(L) = U(0)\exp(-\alpha L)$$
$$= U(0)\exp\left(-\frac{\omega_0}{Q\,v_g}L\right) \quad (5)$$

where v_g is the group velocity of the waveguide mode at frequency ω_0. The propagation loss of the waveguide at ω_0 is therefore given by the ratio of ω_0 and the product of the quality factor Q and the group velocity v_g

$$\alpha = \frac{\omega_0}{Q\,v_g} = \frac{2\pi c/a(a/\lambda_0)}{Q\,v_g}$$
$$= \frac{2\pi n_g}{a\,Q}\left(\frac{a}{\lambda_0}\right) \quad (6)$$

where n_g is the group index of the waveguide mode $n_g = c/v_g$. Group velocity can be generally calculated from the dispersion diagram of the waveguide by $v_g = \partial\omega_0/\partial\beta$. However, such calculations generally require a detailed ω–β dispersion relation at a very small sampling step $\Delta\beta$.

III. SINGLE-LINE DEFECT PHOTONIC CRYSTAL WAVEGUIDES

In this section, we will analyze the propagation loss of five single-line defect photonic crystal waveguides, as detailed in Table I. Of these five, two are suspended membrane structures that differ in their suspension distances above a GaAs substrate. Distance in the normalized thickness $d/a = 1.0$ and 3.0 are considered here. Another two waveguide geometries in which the membranes have asymmetric air-top and oxide-bottom cladding layers are considered with oxide thickness of $d/a = 2.0$ and 5.0. Finally, a deeply etched structure in which the photonic crystal extends through the $Al_xGa_{1-x}As$ lower cladding layer is included. All five structures have a GaAs substrate. It is worth noting that the result from this paper is equally applicable to waveguides fabricated in InP and Si material systems as the refractive indices of each layers can be reproduced in both materials at 1.55 μm. We limit our study to defect waveguides
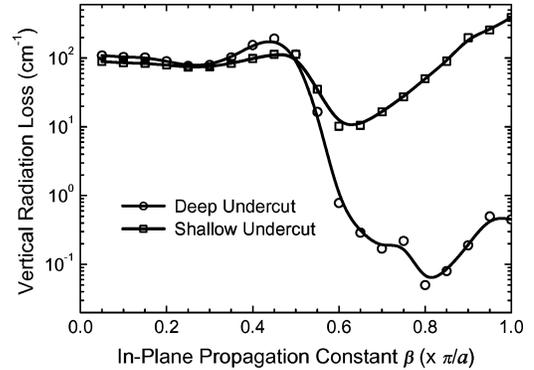
Fig. 3. Vertical radiation loss of the suspended-membrane single-line defect photonic crystal waveguide as a function of the in-plane propagation constant β. The values at the reduced Brillouin zone boundary $\beta = \pi/a$ are not included in the plot to avoid divergence due to the slow wave effect.

formed by removing a single row of holes along the Γ–K direction. In all cases, holes with radii of $r/a = 0.3$ arrayed in a triangular lattice are taken to perforate five dielectric structures.

We only deal with the lowest order even mode in the bandgap that is marked with a thick curve in the dispersion diagram. The out-of-plane transmission loss as a function of the in-plane propagation constant β for the suspended membrane photonic crystal waveguides is plotted in Fig. 3. Since this loss does not include the in-plane radiation loss or that resulting from fabrication imperfections, it should be viewed as a lower limit to the loss expected for real devices. The radiation goes up as the waveguide modes reach above the light line. A thick low-index bottom cladding layer is required for isolating the guided modes from the radiation modes of the substrate. Still, radiation through the bottom cladding generally dominates the out-of-plane radiation loss. The deep undercut structure suffers the least vertical radiation loss among all the waveguides considered and has a minimum loss of approximately $0.2\,\mathrm{cm}^{-1}$ caused by the remaining evanescent coupling between the waveguide mode and the radiation modes of the high-index substrate. Both suspended membrane structures suffer higher loss at the Brillouin zone boundary as a result of a slower group velocity. Comparing with available computational results [12], the propagation loss for the fundamental mode above the light line, which is dominated by the out-of-plane radiation loss, is nearly identical. Below the light line, however, differences appear. Because [12] calculates total (in-plane and out-of-plane) loss of a suspended membrane
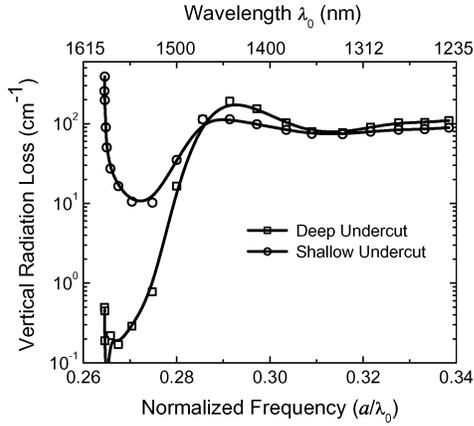
Fig. 4. Vertical radiation loss of suspended membrane single-line defect photonic crystal waveguides as a function of normalized frequency.

photonic crystal waveguide with no high-index substrate in the proximity, the propagation loss is largely due to the in-plane loss caused by a finite number of photonic crystal claddings. In contrast, the below-light-line loss shown in Fig. 3 is the result of the remaining out-of-plane coupling between the waveguide mode and the high-index substrate, which could be significant if membrane is only 0.5 μm above the substrate.

In general, waveguide transmission loss is characterized as a function of frequency or wavelength. This can be obtained by mapping the propagation constant to the corresponding normalized frequency a/λ_0 given by the waveguide dispersion relation. Fig. 4 shows the vertical radiation loss of the waveguide as a function of normalized frequency. The plot covers the frequency range for the guided mode marked as a thick line in Fig. 1. The top axis of the figure also shows that the corresponding wavelength in vacuum had a lattice constant of $a = 450$ nm been taken for the waveguide.

Both suspended-membrane photonic crystal waveguides allow low-loss transmission between normalized frequency of 0.265 and 0.275. However, for the deep undercut structure where the membrane is suspended by 1.35 μm above the GaAs substrate, the lowest out-of-plane radiation loss is 0.2 cm^{-1}. In comparison, the same loss for a shallow undercut structure whose membrane is suspended by only 450 nm is 10 cm^{-1} at its minimum. The out-of-plane radiation loss is improved by 50 times by a moderate increase (900 nm) of the separation between membrane and the substrate. The low-loss bandwidth is approximately 60 nm when operating around 1550 μm as the central working wavelength.

Fig. 5 shows the magnitude of the magnetic field component H_z of the defect waveguide mode at the mid-plane of the membrane for selected propagation constants from π/a to 0. It is extrapolated from the field in a unit cell, calculated from the 3-D FDTD method with an appropriate phase constant

$$H_z(\boldsymbol{r} + \boldsymbol{R}) = H_z(\boldsymbol{r})e^{i\beta R}. \tag{7}$$

The dotted black circles in the plot delineate the edges of the air holes. The corresponding reciprocal space distributions of the modes given by a Fourier transform are shown on the
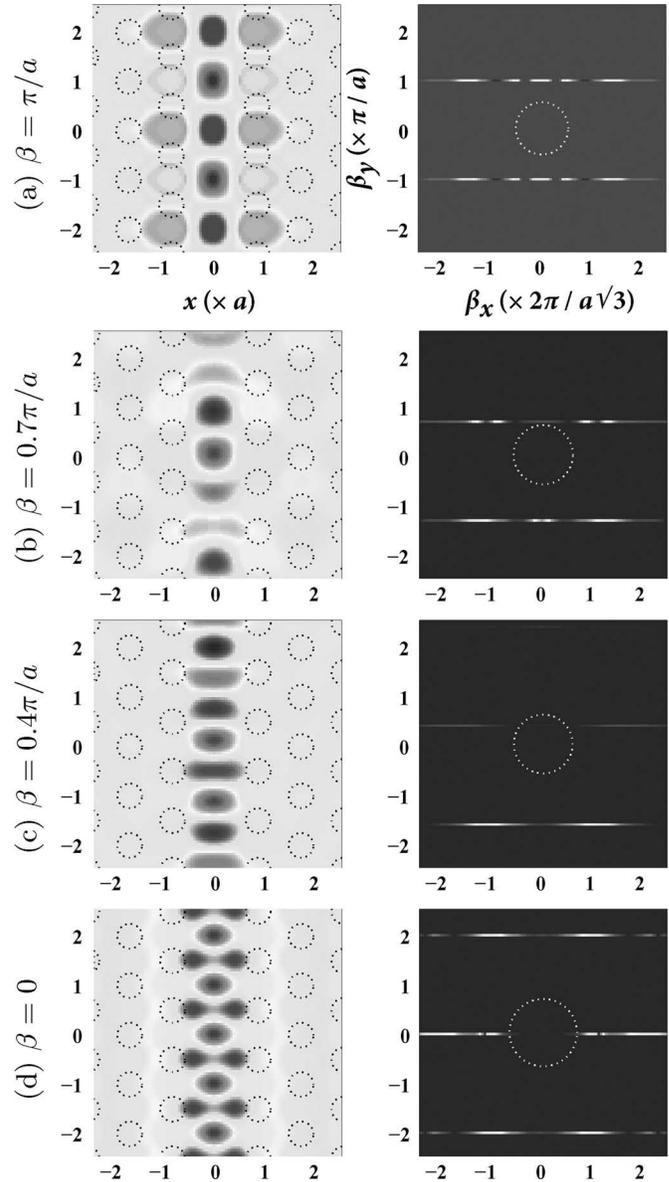
Fig. 5. Propagation mode at the mid-plane of the waveguide slab and their inverse space distribution for the single line-defect photonic crystal waveguides at propagation constant β of (a) π/a, (b) $0.7\pi/a$, (c) $0.4\pi/a$, and (d) 0.

right. A white dashed circle in the middle of the plot shows the projection of the air light line, given by $\sqrt{\beta_x^2 + \beta_y^2} = \omega/c$.

The Fourier transform of the field at $\beta = \pi/a$ shows that it is predominantly distributed at $\beta_y = \pm\pi/a$. In the $\hat{x}$-direction, the reciprocal space distribution spreads out as a result of the lateral confinement. Its distribution in the $\hat{y}$-direction is a delta function. The width shown in the figure is an artifact to enhance the image clarification. Note that there is zero overlap of the mode with the radiation air light line. As shown in Fig. 3, waveguide modes with zero overlap with the light line are practically lossless except for the evanescent coupling loss to the substrate when the membrane is not suspended far enough above the substrate.

Except for the case of $\beta_y = 0$, the predominant spatial harmonics lies in the first extended Brillouin zone $-2\pi/a < \beta_y < -\pi/a$. As shown in Fig. 5, the Bloch part of the waveguide
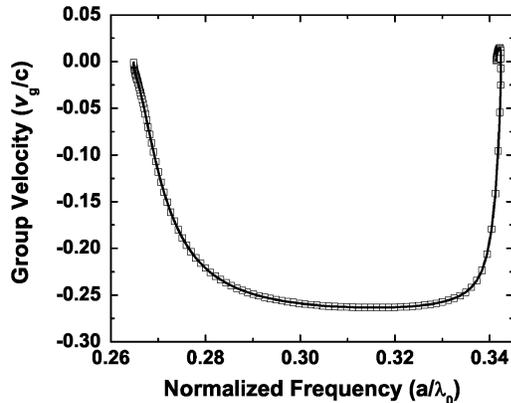
Fig. 6. Group velocity v_g for the lowest waveguide modes in the photonic bandgap of a suspended-membrane photonic crystal defect waveguide.

Fig. 7. Propagation loss of a single-line defect photonic crystal waveguide calculated by the quality factor of the mode, compared with the result from the power method.

mode can be generally approximated by the sum of the two spatial harmonics. As the in-plane propagation constant β of the waveguide mode varies from π/a to 0, its spatial harmonic in the first Brillouin zone, $-\pi/a < \beta_y < \pi/a$, becomes increasingly closer to the radiation light cone and eventually overlaps. As shown in Fig. 3, the out-of-plane radiation loss increases dramatically at $\beta = 0.5\pi/a$. It corresponds to the waveguide mode whose reciprocal space distribution first overlaps with the light cone. The close correlation of the out-of-plane radiation loss of the waveguide mode and its reciprocal space distribution suggests that the propagation loss can be reduced by decreasing the mode overlap with the radiation light cone. However, it should be noted that the out-of-plane radiation loss is the Poynting vector flux of the electromagnetic field away from the guiding layer. The Fourier transform of the magnetic field at the center of the slab only gives a qualitative estimate of the waveguide loss. In Section IV, waveguide with an improved out-of-plane loss is designed under such premise.

As stated in Section II, the propagation loss of photonic crystal waveguide can also be calculated by the quality factor method. Fig. 6 shows the group velocity for the defect mode of interest for the suspended membrane photonic crystal waveguide. It is obtained from a 3-D finite-element method (FEM) [4]. The sign of its value is only a matter of choice in the calculation and should not be taken as a negative index behavior. As can be seen in the figure, the group velocity for a broad range of normalized frequency between 0.29 and 0.33 is nearly constant. However, it decreases dramatically as the mode approaches the Brillouin zone boundary, implying a slow wave behavior. It is worth noting that the results given by the 3-D FEM is likely to be different from those of the 3-D FDTD, had we decided to calculate the group velocity with 3-D FDTD. This is partly due to the distinction in their approaches for numerical discretization. FEM applies triangulation, which usually conforms better to the circular geometry than do cartesian grids employed in FDTD, under the same mesh density. Later, in comparing the transmission loss from quality factor method with the power ratio method, we should bear in mind that v_g attributes to the discrepancy to some extent.
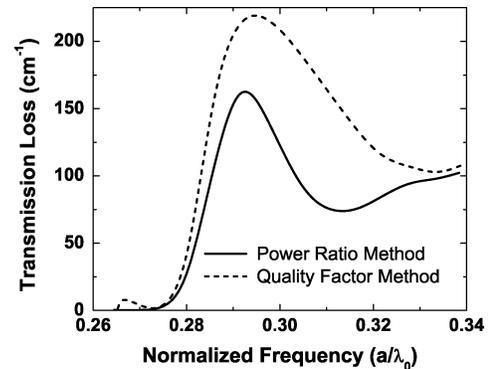
The propagation loss for the same mode in Figs. 3 and 4 can be calculated from its quality factor and group velocity by applying (6). The method for calculating the quality factor is detailed in [14]. The waveguide modes at the reduced Brillouin zone boundary $\beta = \pi/a$ and $\beta = 0$ are removed from the calculation due to the difficulty with respect to their group velocity. Their theoretically zero group velocity [28] often makes numerical result insensible. Fig. 7 shows the transmission loss of the waveguide mode as a function of the normalized frequency using both the power ratio and the quality factor methods. However, the result from the power ratio method only includes the loss as a result of the out-of-plane radiation, therefore the quality factor method always gives a slightly higher transmission loss.

A remarkable agreement can be found from the results given by both approaches for the normalized frequency a/λ_0 less than 0.28. It corresponds to low-loss transmission for the waveguide. Both methods predict a minimum transmission loss of a fraction of 1 cm^{-1}. The discrepancy increases as the defect waveguide mode moves above the radiative light line. Intuitively, we would expect that the out-of-plane radiation loss dominates the total loss for such lossy modes and therefore lesser discrepancy between two methods. This seeming contradiction arises from the definition of the out-of-plane radiation loss. It is taken as optical power exiting the top and bottom domains. However, the defect mode above the light line apparently radiates at a large angle in the case of uniform air cladding. A portion of the power that is considered as the in-plane radiation loss is, *in fact*, due to the out-of-plane radiation. Even so, the trend for $a/\lambda_0 > 0.28$ for both methods is similar.

The advantage of calculating the propagation loss from the waveguide modes' quality factor is obvious. It does not require an additional full 3-D FDTD simulation. The waveguide transmission properties are practically given at the same time as the dispersion band diagram. Of course, it cannot give us the waveguide mode distribution due to the removal of the additional simulation. Additionally, the quality factor method cannot distinguish the out-of-plane transmission loss from the in-plane loss directly. However, such information can, in general, be inferred from the dispersion band diagram.
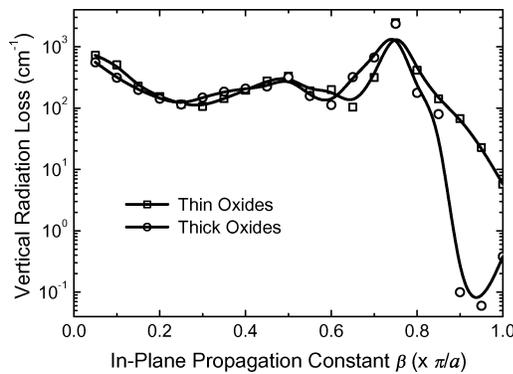
Fig. 8. Vertical radiation loss of oxide lower cladding single-line defect photonic crystal waveguide as a function of the in-plane propagation constant.

Fig. 9. Vertical radiation loss of oxide lower cladding single-line defect photonic crystal waveguide as a function of normalized frequency.

Fig. 10. Vertical radiation loss as a function of normalized frequency for a low index contrast single-line defect photonic crystal waveguide on an epitaxial structure.

Even though suspended-membrane photonic crystal waveguides offer a broad bandwidth for low-loss operation, its prospect as the basic building block for integrated optical device is clouded by several issues. First of all, efficient current injection into the suspended membrane structure is difficult. Since the membrane is surrounded by electrical insulators vertically, lateral current injection is usually required. Air is not only an electrical insulator, but also a thermal insulator. For nonlinear applications where high optical power density is required, concern is raised for suspended-membrane photonic crystal waveguides as to whether they are capable of channeling the heat. In addition, power coupling with other optical components on high-index substrate is likely to cause significant reflection. The mechanical stability of the membrane waveguide is also questionable, particularly for devices with a large dimension.

For the aforementioned reasons, efforts are made to create low-loss photonic crystal waveguide on a high-index substrate. Since the radius of the substrate light cone is proportional to its refractive index, optical materials with the smallest dielectric constant are preferred. Considering the ease of fabrication integration, Al_xO_y or sapphire naturally becomes the best candidate. Aluminum oxide, which has a refractive index of 1.6, is formed by oxidizing $Al_xGa_{1-x}As$ with high Al composition. Sapphire, on the other hand, can be bounded onto the GaAs epitaxial structure [29]. Both structures are referred in the later context as oxidized lower cladding.

The vertical radiation loss of such photonic crystal waveguides is shown in Figs. 8 and 9 as a function of propagation constant and normalized frequency, respectively. As in the case with the suspended-membrane photonic crystal waveguides, a thicker oxide cladding yields lower out-of-plane radiation loss.

In comparison with the suspended-membrane photonic crystal waveguide, the range of wave vectors under the cladding light line is greatly reduced due to a lower index contrast between the guiding layer and the bottom cladding. That range, which is in the vicinity of the Brillouin zone boundary, also corresponds to the low group velocity region. Consequently, oxidized lower cladding structures allow a much narrower bandwidth, less than 3 nm near 1550 nm in this case. However, by tuning the waveguide structure by means of the defect width, hole radius, and hole shape, a broader bandwidth for an oxidized lower cladding or sapphire-clad defect waveguide can be obtained [30].
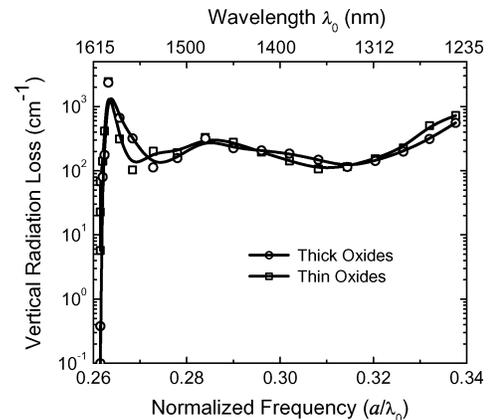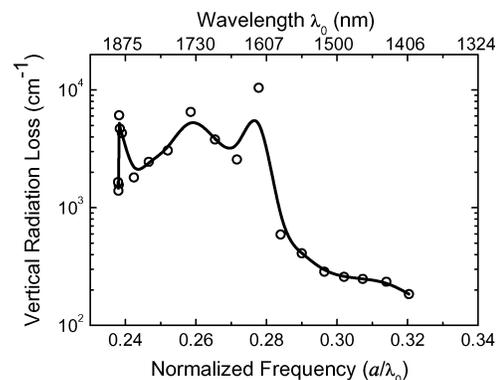
Beside placing guiding membrane on an oxide cladding, photonic crystal waveguide is also created from low index contrast epitaxial structure. The air holes usually perforates the semiconductor by a few micrometers. Due to a weak vertical index contrast, transmission loss for single-line defect photonic crystal waveguides on an epitaxial structure is very high. Fig. 10 shows the out-of-plane radiation loss for the deeply etched photonic crystal waveguides. The lattice constant a is chosen to be 480 nm. As can be seen from the plot, loss is generally high, because the Bloch mode is above the substrate light line for all the propagation constants. This waveguide is predicted to have a minimum out-of-plane radiation loss of 174 cm^{-1}. The operation range, in which this loss is predicted to be 300 cm^{-1} when centered at 1550 nm, spans a wavelength range of 134 nm. This range corresponds to the modes near the vicinity of the Brillouin zone center in the reciprocal space.

It should also be noted that deeply etched waveguides formed by removing multiple rows of holes have been demonstrated with significantly lower radiation loss. The calculations indicate that a reduction in the radiation loss by more than three orders of magnitude for these structures is possible. However, these waveguides are multimoded at all frequencies.
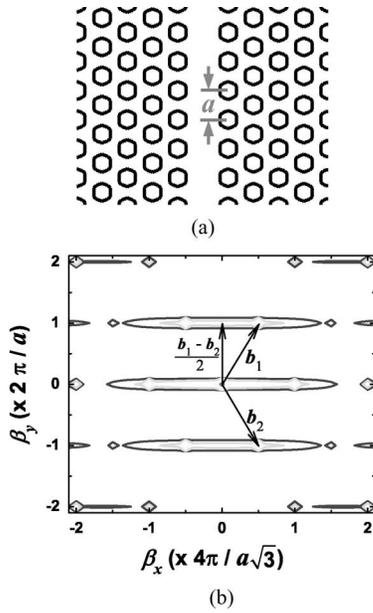
Fig. 11.   (a) In-plane dielectric distribution of the waveguide and (b) its Fourier transform for a single-line photonic crystal defect waveguide. The adjacent color levels in the contour differ in magnitude by a decade.

Fig. 12.   (a) In-plane dielectric distribution of photonic crystals. (b) Its Fourier transform. The adjacent color levels in the contour differ in magnitude by a decade.

IV. TYPE-B PHOTONIC CRYSTAL WAVEGUIDE

In Section III, we have shown that the propagation loss of the photonic crystal waveguides is strongly influenced by the vertical index profile. As shown in Fig. 5, the waveguide mode is primarily consisted of two spatial harmonics, one of which is within the range β_y of $-\pi/a$ and π/a. As the radiation light cone enlarges due to a higher refractive index of the bottom cladding, the spectral range in which spatial harmonics do not overlap with the radiation light cone is reduced. For the case of a deeply etched photonic crystal waveguide, all waveguide modes in the photonic bandgap have substantial amount of overlap with the radiation light cone of the bottom cladding. The resulting coupling with the radiation modes leads to a propagation loss of over 100 cm^{-1}; whereas, for suspended membrane and oxidized lower cladding photonic crystal waveguides, a propagation loss of 1 cm^{-1} or less can be achieved for those modes that have no spatial harmonics inside the radiation light cone. It can, therefore, be expected that the out-of-plane radiation loss can be reduced by decreasing the overlap of the waveguide mode and the radiation light cone. In this section, we will first analyze the role of the photonic crystals played in forming the waveguide mode and then present an approach to reduce the out-of-plane radiation loss for photonic crystal waveguide with low vertical index contrast.

Fig. 11 shows the in-plane dielectric distribution of the waveguide in real and reciprocal spaces. The reciprocal space distribution of the dielectric is obtained from a Fourier transform of the real space distribution, which is *not* shown in full in Fig. 11. The periodicity of the distribution in real space is very critical to accurately calculating the reciprocal distribution. Not only does the inter-hole spacing have to be precisely *identical*, the boundaries of the real space lattice also *must* satisfy periodicity as is assumed in the fast Fourier transform (FFT). For the vertical
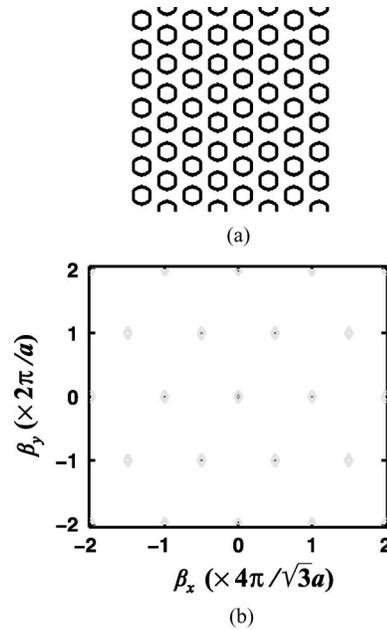
direction of the figure, the distance between neighboring holes ΔO_y equals to the lattice constant a; whereas, for the horizontal direction, that distance ΔO_x is given by an irrational fraction of a lattice constant $\sqrt{3}a/2$. Because of the strict requirement of periodicity, the differential spacing Δx for the horizontal direction is intentionally modified to be an integer n_x division of ΔO_x. This allows the distance between neighboring circles to be an exact integer, free from the rounding error in a floating point number. Since the scaling of the horizontal and vertical directions are different, the Fourier transform shall be inversely scaled to reflect the actual result.

With the preceding procedures, the reciprocal space distribution of a perfect photonic crystal lattice is given by discrete points at the lattice point as shown in Fig. 12. The contour plot shows that nonzero Fourier components are expected only at the reciprocal lattice locations. It is worth noting that the contours do not have a physical width. The radius of each delta component is an artifact to improve the clarification of the plot.

As shown in Fig. 11(b), the presence of the missing row of holes causes spatial Fourier components that would not be present in a bulk 2-D triangular lattice. In particular, there are Fourier components along the waveguide direction, $\Gamma-K$, at $(\boldsymbol{b}_1 - \boldsymbol{b}_2)/2$, where $\boldsymbol{b}_1$ and $\boldsymbol{b}_2$ are primitive vectors of the reciprocal lattice.

From the discrete translation invariance of the waveguide along the propagation direction and the Fourier transform of the lattice, the electric field in the waveguide can be written as

$$\boldsymbol{E}(x,y,z,t) = \sum_n c_n \boldsymbol{f}_\beta(x,z)$$

$$\times \exp\left(i\left\{\omega t - \left[\beta + n\left(\frac{\boldsymbol{b}_1 - \boldsymbol{b}_2}{2}\right)\right]y\right\}\right) \quad (8)$$

(a)

(b)
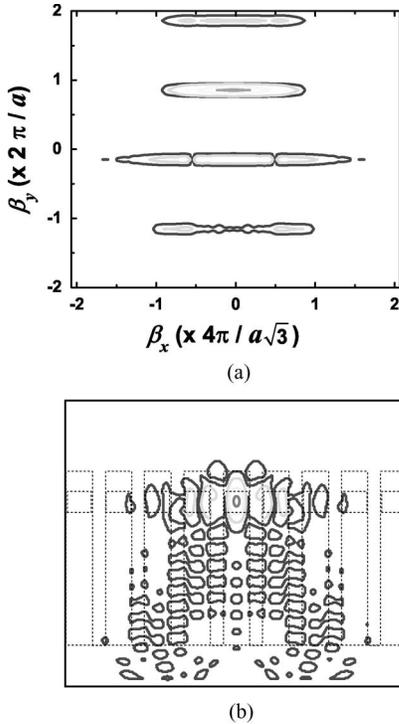
Fig. 13. (a) Fourier transform of H_z at the mid-plane for the defect waveguide mode at $\beta_y = 0.2\pi/a$. (b) H_z^2 shown in the cross section of the same mode with waveguide dielectric distribution overlaid by *dotted lines*. The adjacent color levels differ in magnitude by a decade.

where n is an integer and c_n is the coefficient for the spatial harmonics. β is restricted to the first Brillouin zone of the reciprocal space. Given b_1 and b_2 shown in Fig. 11(b), it can be shown that

$$\frac{b_1 - b_2}{2} = \frac{2\pi}{a}\hat{\beta}_y. \tag{9}$$

The field solution assumed in (8) agrees with the reciprocal space distribution of the waveguide mode shown in Fig. 5. As can be seen in the figure, only the $n = 0$ term c_0 in this series is inside the radiation cone of the cladding layers and contributes to the radiation loss of the waveguide mode.

This term is not large, however, as can be seen from Fig. 13(a), which shows the Fourier transform of the in-plane H_z component for the same propagation constant $\beta_y = 0.2\pi/a$ as field H_z^2 in Fig. 13(b) obtained from a 3-D FDTD simulation. It shows that the dominant component of the field is c_1, which is in the second zone. c_1 is outside the light cone and does not contribute to the radiation loss of the waveguide mode. c_1 and c_0 are coupled by the Fourier component of the lattice at $(b_1 - b_2)/2$. It is clear that not only does the field leak through the photonic crystal cladding but also the mode actually has strong vertical propagation directly beneath the waveguide core that contributes to the out-of-plane radiation loss. This can be identified in Fig. 13(b) by the multiple contours in $Al_x Ga_{1-x} As$ cladding aligned below the defect. It implies an oscillatory, or traveling wave behavior of the electromagnetic field. For a rigorous waveguide confinement, we expect the field magnitude to exponentially decay in the waveguide cladding and substrate.
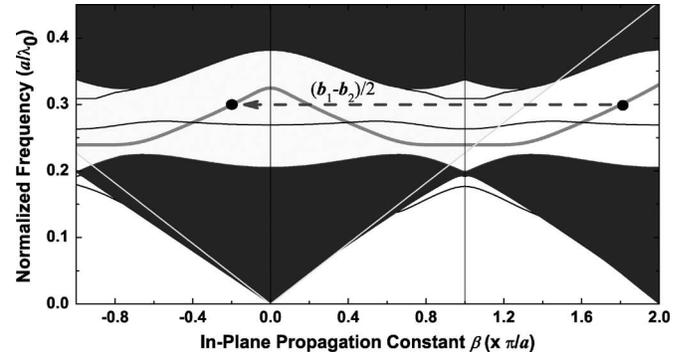
Fig. 14. Photonic band diagram for a deeply etched single-line photonic crystal defect waveguide, described in Table I, in an extended Brillouin zone scheme. The defect mode analyzed for out-of-plane radiation loss is marked as a *bold line*.

Fig. 14 shows the photonic band diagram of a deeply etched photonic crystal waveguide in an extended Brillouin zone scheme. The vertical radiation light cone due to the bottom cladding and transverse radiating region in the photonic crystal are mapped as yellow and dark blue areas, respectively. The defect modes of interest for the out-of-plane radiation loss analysis are marked with a thick curve in the figure. It is clear that the waveguide mode is completely inside the radiation light cone of the bottom cladding.

Two of the spatial harmonics in the range of $-\pi/a < \beta_y < 2\pi/a$ in Fig. 13 are identified in Fig. 14. The $n = 0$ and $n = 1$ terms, c_0 and c_1, in the c_n of (8) are marked in the figure. They are separated by $G = 2\pi/a$. If we take the average index of the photonic crystal waveguide, the propagation constant of the resulting waveguide mode can be estimated by the product of the effective mode index n_{eff} and free-space wavenumber $k_0 = 2\pi/\lambda_0$. In the case of a deeply etched photonic crystal waveguide, the mode has a propagation constant of $0.9 \times 2\pi/a$ assuming an effective index of 3 and normalized frequency of $a/\lambda_0 = 0.3$. It is in the second Brillouin zone. Drawing an analogy with the coupled mode theory, the spatial harmonics of the photonic crystal waveguide mode in the first Brillouin zone is the result of the coupling by the lattice G.

If the coupling between the $n = 0$ component in the field in (8) and the $n = 1$ component is reduced by reducing or eliminating the Fourier component of the lattice at $(b_1 - b_2)/2$, so is the waveguide radiation loss. This can be accomplished in a type-B photonic crystal waveguide, which is formed by removing a single row of holes from a triangular lattice and then shifting one side of the cladding along the direction of the waveguide by half a lattice period. For convenience, we will refer the conventional photonic crystal waveguides as type-A waveguides.

Fig. 15(a) shows the in-plane dielectric distribution of a type-B waveguide and its Fourier transform is shown in Fig. 15(b). Photonic crystals both to the left and right sides of the linear defect are triangular lattice with the same lattice constant and hole radius. The position of the cladding is however displaced by half a period. It shows that there is no Fourier component of the lattice along $\Gamma - K$ at $(b_1 - b_2)/2$ because of the cancelation of the contributions from each side of the cladding after the half-period shift.
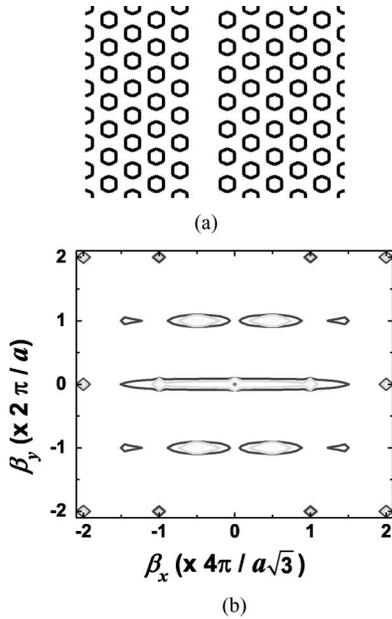
Fig. 15. (a) In-plane dielectric distribution of the waveguide and (b) its Fourier transform for a type-B single-line photonic crystal defect waveguide. The adjacent color levels differ in magnitude by a decade.

Fig. 16. Photonic band diagram for a type-B photonic crystal waveguide on an epitaxial structure consistent with $Al_x Ga_{1-x} As/GaAs/Al_x Ga_{1-x} As$. The defect mode analyzed for the out-of-plane radiation loss is marked by the *thick curve*. The *dark gray* and *light gray* regions indicate the modes of the bulk photonic crystals and vertical radiation light cone.

We expect a reduced radiation loss in a type-B waveguide because of the elimination of the Fourier component at $(\boldsymbol{b}_1 - \boldsymbol{b}_2)/2$, which occurs along the $\Gamma-K$ axis, where the Fourier transform of the field is peaked. In addition, radiation loss is further reduced because the radiation field under the two waveguide cladding sections is out of phase because of the spatial shift in the lattice leading to a cancelation under the waveguide core.

Fig. 14 shows the dispersion relation of a type-B waveguide. The dark blue and light yellow areas represent the regimes where the electromagnetic field radiates in the photonic crystal cladding and radiates out-of-plane, respectively. The waveguide mode of interest is marked with thick curve in the figure. Except for the propagation constant β smaller than $0.4\pi/a$ where anti-crossing between the lowest two modes occurs, the magnetic field component H_z of this mode assumes an even-like symmetry along the center of the waveguide.

In type-A structures, the photonic crystal cladding has even symmetry along the center of the defect. If the photonic crystal is thought of as a perturbation of an epitaxial waveguide structure, the coupling of a laterally even mode and a laterally odd mode under an even symmetry perturbation is zero. As shown in Fig. 16, the lowest waveguide mode in the photonic bandgap, which assumes even symmetry, intersects with the next higher mode, which assumes odd symmetry. However, the perturbation is neither strictly even nor odd in a type-B waveguide, resulting in an anti-crossing at the frequency where the even and odd modes would otherwise intercept. Because of the anti-crossing, the lowest mode of the propagation constant between 0 and $0.4\pi/a$ possesses an odd-like symmetry, which is the symmetry property of the next higher mode in the bandgap.

Another distinction for type-A and type-B band diagrams is at the Brillouin zone boundary. For type-A photonic crystal waveguides, the dielectric distribution at $\beta_y = 2\pi/a$ causes degeneracy breaking for all modes at a propagation constant β_y of π/a. However, due to the cancelation of out-of-phase photonic crystals at $\beta_y = 2\pi/a$, the waveguide mode at the Brillouin zone boundary is nearly degenerate. A slight frequency split does exist since this Fourier component is only zero along the $\Gamma-K$ axis as shown in Fig. 15(b) and the Fourier transform of the mode in this waveguide has some spread in the β_x and β_z directions because of the confined transverse mode profile $f_\beta^{(B)}(x,z)$.

Fig. 17 shows the magnitude of the magnetic field component H_z and its reciprocal space intensity distribution for the propagation modes in a single-line type-B photonic crystal waveguide. The 2-D intensity plots only show the field at the mid-plane of the guiding layer for the lowest propagation mode in the photonic bandgap, which is marked with bold lines in Fig. 16. As the epitaxy on which the photonic crystal waveguides is created has a nearly symmetrical index profile with respect to the guiding layer, the magnetic field is expected to be predominantly H_z at the mid-plane of the guiding layer for the TE_z mode. It is justified to use single H_z component to analyze the properties of the mode. The dashed circle in the reciprocal space represents the light line. Because photonic crystals extend a few micrometers into the bottom cladding, the radiation light cone is strongly modified by the presence of the periodic structure similar to the case of out-of-plane propagation in the 1-D periodic layers. The radius of the light line is chosen to reflect the average index of the bottom cladding.

As shown in Fig. 16, the lowest propagation mode in the photonic bandgap intersects with the band of the photonic crystals around the propagation constant of $0.8\pi/a$ and higher. The lateral confinement of the field suffers as a result of the interaction of the photonic crystal cladding. However, the weak spatial confinement results in a strong confinement in the reciprocal space. The field distribution in the reciprocal space have the smallest spread around the lattice points as shown in Fig. 17(a). Even though the out-of-plane radiation loss of this mode is small, the strong coupling with the photonic crystal cladding mode nevertheless makes it an overall poor candidate for waveguiding.
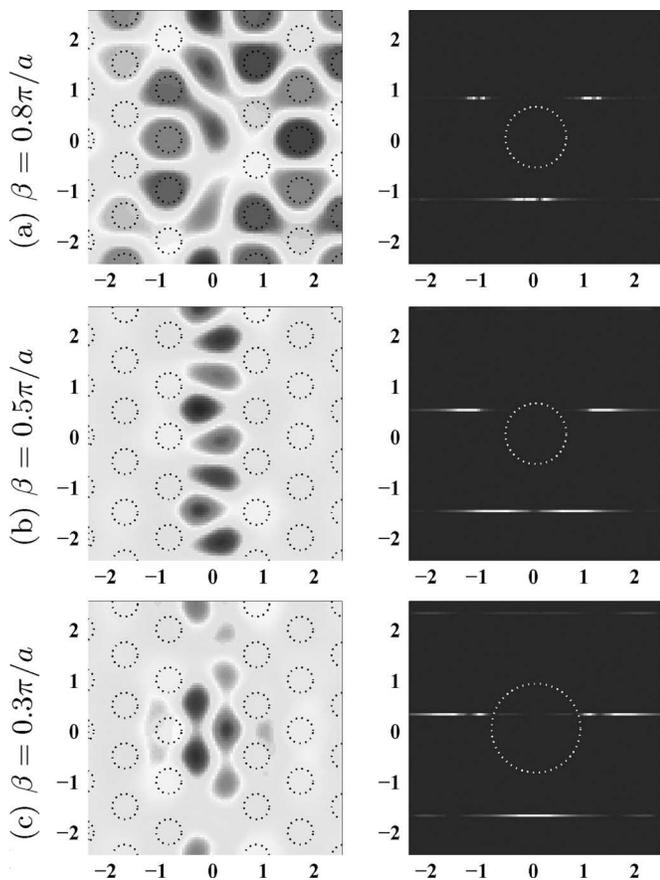
Fig. 17. Propagation mode at the mid-plane of a type-B photonic crystal waveguide and their inverse space distribution for single-line defect photonic crystal waveguides at various values of the propagation constant β. (a) $0.8\pi/a$. (b) $0.5\pi/a$. (c) $0.3\pi/a$.
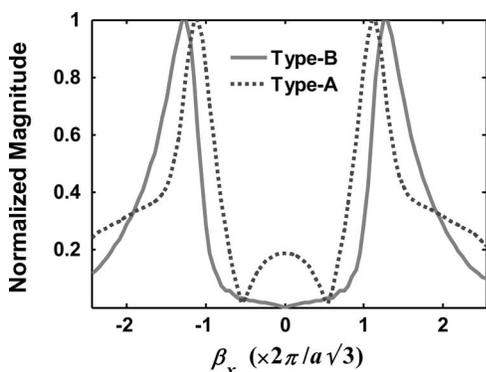
Fig. 18. Reciprocal space distribution of type-A and type-B photonic crystal defect waveguide mode at $\beta = 0.6\pi/a$ and $\beta = 0.5\pi/a$, respectively.

Fig. 18 shows the spatial harmonics of type-A and type-B photonic crystal waveguide modes in the first Brillouin zone. Both plots are normalized with their peak magnitude. The propagation constants for the type-A and type-B waveguide modes are $0.6\pi/a$ and $0.5\pi/a$, respectively. It agrees with our previous analysis that the coupling between the spatial harmonics is directly linked to the reciprocal space distribution of the waveguide lattice. By removing the Fourier component of the lattice along Γ–K at $(\boldsymbol{b}_1 - \boldsymbol{b}_2)/2$, the spatial harmonics for the type-B
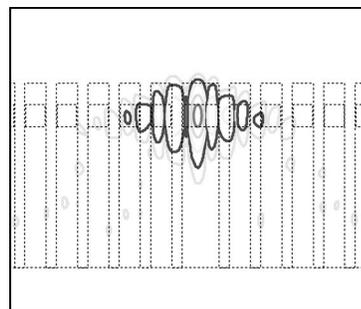
Fig. 19. H_z^2 field cross section for the type-B photonic crystal defect waveguide mode at $\beta_y = 0.5\pi/a$. The *dotted lines* outline the waveguide dielectric distribution. The field contour has one additional color level compared with Fig. 13(b) to identify the radiation path. The adjacent color levels differ in magnitude by a decade.

waveguides is zero at $\beta_x = 0$. The magnitude at the vicinity of $\beta_x = 0$ is also small. In comparison, the magnitude for type-A waveguide modes is much stronger at the same location. Because the part that overlaps with the radiation light cone has predominantly small β_x, type-B waveguides have a smaller out-of-plane radiation loss.

Fig. 19 shows the longitudinal cross section of H_z^2 of the guided modes in the type-B waveguides at $0.5\pi/a$. The epitaxial structure and the air hole positions are delineated in the figure as dashed lines. A comparison with the type-A waveguide mode at $0.2\pi/a$ can be found in Fig. 13. This will be shown to be the point with the lowest out-of-plane radiation loss for the band considered. As shown in the figure, the vertical propagation beneath the linear defect is absent. Radiation loss underneath each of the cladding sections remains but is reduced. However, the vertical attenuation of a type-B waveguide mode is slower than that of a type-A waveguide. For a type-A suspended membrane photonic crystal waveguide, the field decays over an order of magnitude from the mid-plane of the guiding membrane to the cladding interface. And that for a type-B photonic crystal waveguide is less than a factor of 4. Because of that, holes must be deeply etched in type-B structures to prevent the waveguide modes from coupling with the radiation modes of the substrate.

The out-of-plane radiation loss as a function of normalized frequency for type-B photonic crystal single-line defect slab waveguides is shown in Fig. 20. The epitaxial structure of the waveguide and etching depth of the holes are identical with that of the deeply etched photonic crystal waveguide shown in Table I. It is so chosen that a fair comparison of the waveguide transmission loss before and after the optimization can be achieved.

The lowest radiation loss for the type-B defect waveguide with an identical vertical index contrast is predicted to be 10.7 cm^{-1}. Fig. 20 shows the vertical radiation loss of the type-B waveguide as a function of normalized frequency a/λ_0 for a lattice constant of 380 nm. The open squares are the calculation results by the power ratio method following a 3-D FDTD simulation, and the curve is the spline fit. The top axis of the figure shows the corresponding physical wavelength λ_0. The lattice constant for type-B waveguide is chosen to be 70 nm shorter than that of the waveguide in Fig. 10 because the low-loss
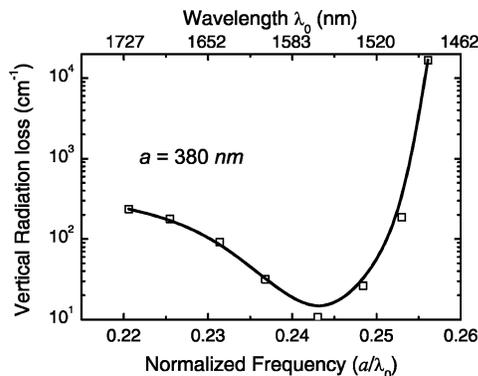
Fig. 20.   Vertical radiation loss for the type-B single-line defect photonic crystal waveguide as a function of normalized frequency.

transmission happens at a slightly lower normalized frequency for the former. As optical communication applications generally require the working wavelengths aligned with 1550 nm low-loss fiber transmission window, we have insisted to have low-loss transmission centered at 1550 nm.

V. Conclusion

In summary, a full 3-D numerical model was developed to analyze the out-of-plane propagation loss of linear defect photonic crystal slab waveguides. An infinite waveguide is emulated by enforcing a periodic boundary condition over the waveguide unit cell. The propagation mode is excited with double orthogonal excitation and a time-domain band-pass filter. The out-of-plane radiation can be calculated either by the ratio of power loss to propagating power or the quality factor of the waveguide mode. The results show that, for a sufficiently thick bottom cladding layer, both the suspended-membrane and oxidized lower cladding structures are capable of low-loss transmission over a range of frequencies. The role of photonic crystals in forming waveguide modes is also examined. We have shown that the out-of-plane radiation loss of the photonic crystal defect waveguide can be reduced by an order of magnitude by shifting the photonic crystal claddings one-half period with respect to each other along the propagation direction.

References

[1] T. Baba, N. Fukaya, and Y. Yonekura, "Observation of light propagation in photonic crystal optical waveguides with bends," *Electron. Lett.*, vol. 35, pp. 654–655, 1999.

[2] S. G. Johnson, S. Fan, P. R. Villeneuve, and J. D. Joannopoulos, "Guided modes in photonic crystal slabs," *Phys. Rev. B, Condens. Matter*, vol. 60, pp. 5751–5758, 1999.

[3] A. Chutinan and S. Noda, "Waveguides and waveguide bends in two-dimensional photonic crystal slabs," *Phys. Rev. B, Condens. Matter*, vol. 62, pp. 4488–4492, 2000.

[4] W. J. Kim, "Full vectorial finite element analysis of photonic crystal devices: Application to low-loss modulator" Ph.D. dissertation, Univ. Southern California, Los Angeles, CA, 2004.

[5] T. N. Langtry, A. A. Asatryan, L. C. Botten, C. M. de Sterke, R. C. McPhedran, and P. A. Robinson, "Effects of disorder in two-dimensional photonic crystal waveguides," *Phys. Rev. E, Stat. Phys. Plasmas Fluids Relat.*, vol. 68, no. 2, p. 026611-1, 2003.

[6] W. Bogaerts, P. Bienstman, and R. Baets, "Scattering at sidewall roughness in photonic crystal slabs," *Opt. Lett.*, vol. 28, no. 9, pp. 689–691, 2003.

[7] S. Hughes, L. Ramunno, J. Young, and J. E. Sipe, "Extrinsic optical scattering loss in photonic crystal waveguides: Role of fabrication disorder and photon group velocity," *Phys. Rev. Lett.*, vol. 94, no. 3, art. no. 033903, 2005.

[8] B. D'Urso, O. Painter, J. O'Brien, T. Tombrello, A. Yariv, and A. Scherer, "Modal reflectivity in finite-depth two-dimensional photonic-crystal microcavities," *J. Opt. Soc. Amer. B, Opt. Phys.*, vol. 15, pp. 1155–1159, 1998.

[9] M. Palamaru and P. Lalanne, "Photonic crystal waveguides: Out-of-plane losses and adiabatic modal conversion," *J. Appl. Phys.*, vol. 78, no. 11, pp. 1466–1468, 2001.

[10] P. Lalanne and H. Benisty, "Out-of-plane losses of two-dimensional photonic crystal waveguides: Electromagnetic analysis," *J. Appl. Phys.*, vol. 89, no. 2, pp. 1512–1514, 2001.

[11] P. Lalanne, "Electromagnetic analysis of photonic crystal waveguides operating above the light cone," *IEEE J. Quantum Electron.*, vol. 38, no. 7, pp. 800–803, Jul. 2002.

[12] C. Sauvan, P. Lalanne, J. Rodier, J. Hugonin, and A. Talneau, "Accurate modeling of line-defect photonic crystal waveguides," *Photon. Technol. Lett.*, vol. 15, no. 9, pp. 1243–1245, 2003.

[13] G. R. Hadley, "Out-of-plane losses of line-defect photonic crystal waveguides," *IEEE Photon. Technol. Lett.*, vol. 14, no. 5, pp. 642–644, May 2002.

[14] W. Kuang, J. R. Cao, S.-J. Choi, J. D. O'Brien, and P. D. Dapkus, "Classification of modes in suspended membrane 19-missing-hole photonic crystal microcavities," *J. Opt. Soc. Amer. B, Opt. Phys.*, vol. 22, no. 5, pp. 1092–1099, 2005.

[15] W. Kuang, C. Kim, A. Stapleton, W. J. Kim, and J. D. O'Brien, "Calculated out-of-plane transmission loss for photonic-crystal slab waveguides," *Opt. Lett.*, vol. 28, pp. 1781–1783, 2003.

[16] W. Kuang and J. D. O'Brien, "Reducing the out-of-plane radiation loss of photonic crystal waveguides on high-index substrates," *Opt. Lett.*, vol. 29, pp. 860–862, Apr. 2004.

[17] K. S. Yee, "Numerical solution of initial boundary vlaue problems involving Maxwell's equation in isotropic media," *IEEE Trans. Antennas Propag.*, vol. AP-14, no. 3, pp. 302–307, May 1966.

[18] A. Taflove and S. C. Hagness, *Computational Electrodynamics: The Finite-Difference Time-Domain Method.*   Norwood, MA: Artech House, 2000.

[19] W. Gropp, E. Lusk, and A. Skjellum, *Using MPI: Portable Parallel Programing with the Message-Passing Interface.*   Cambridge, MA: MIT Press, 1999.

[20] W. Gropp, E. Lusk, and R. Thakur, *Using MPI-2: Advanced Features of the Message-Passing Interface.*   Cambridge, MA: MIT Press, 1999.

[21] J.-P. Berenger, "Perfectly matched layer for the fdtd solution of wave-structure interaction problems," *IEEE Trans. Antennas Propag.*, vol. 44, no. 1, pp. 110–117, Jan. 1996.

[22] C. Chan, Q. Yu, and K. Ho, "Order-n spectral method for electromagnetic-waves," *Phys. Rev. B*, vol. 51, no. 23, pp. 16635–16642, 1995.

[23] M. Celuch-Marcysiak and W. Gwarek, "Spatially looped algorithms for time-domain analysis of periodic structures," *IEEE Trans. Microw. Theory Tech.*, vol. 43, no. 4, pp. 860–865, Apr. 1995.

[24] A. V. Oppenheim and R. W. Schafer, *Discrete-Time Signal Processing.* Englewood Cliffs, NJ: Prentice-Hall, 1989.

[25] S. Dey and R. Mittra, "Efficient computation of resonant frequencies and quality factors of cavities via a combination of the finite-difference time-domain technique and the pade approximation," *IEEE Microw. Guided Wave Lett.*, vol. 8, no. 12, pp. 415–417, Dec. 1998.

[26] W.-H. Guo, W.-J. Li, and Y.-Z. Huang, "Computation of resonant frequencies and quality factors of cavities by FDTD technique and pade approximation," *IEEE Microw. Wireless Compon. Lett.*, vol. 11, no. 5, pp. 223–225, May 2001.

[27] A. Yariv, *Optical Electronics in Modern Communications*, 5th ed. Oxford: Oxford Univ. Press, 1997.

[28] M. Notomi, K. Yamada, A. Shinya, J. Takahashi, C. Takahashi, and I. Yokohama, "Extremely large group-velocity dispersion of line-defect waveguides in photonic crystal slabs," *Phys. Rev. Lett.*, vol. 87, pp. 253902-1–253902-4, 2001.

[29] J. R. Cao, Z.-J. Wei, W. Kuang, S.-J. Choi, H. Yu, J. D. O'Brien, and P. D. Dapkus, "Sapphire-bonded photonic crystal microcavity lasers and their far-field radiation patterns," *Photon. Technol. Lett.*, vol. 17, no. 1, pp. 4–6, 2005.

[30] M. Notomi, A. Shinya, K. Yamada, J. Takahashi, C. Takahashi, and I. Yokohama, "Structural tuning of guiding modes of line-defect waveguides of silicon-on-insulator photonic crystal slabs," *IEEE J. Quantum Electron.*, vol. 38, no. 7, pp. 736–742, Jul. 2002.

Wan Kuang (S'02–M'06) received the B.S.E.E. and M.S.E.E. degrees from Chongqing University of Posts and Telecommunications, Chongqing, China, and the Ph.D. degree from the University of Southern California, Los Angeles, all in electrical engineering.

Currently, he is an Assistant Professor in the Department of Electrical and Computer Engineering, Boise State University, Boise, ID. His research interests include numerical methods in electromagnetics and photonic bandgap material.

Woo Jun Kim received the Ph.D. degree in electrical engineering from the University of Southern California, Los Angeles.

Adam Mock was born in Oklahoma City, OK, in 1980. He received the B.S. degree in electrical engineering from Columbia University, New York, NY, in 2003. Currently, he is working toward the Ph.D. degree in electrical engineering in the MicroPhotonics Research Group, University of Southern California, Los Angeles.

His research interests include numerical electromagnetic modeling of photonic crystal devices.

John O'Brien (M'98–SM'02) received the B.S. degree in electrical engineering in 1991 from Iowa State University, Ames. He received the M.S. and Ph.D. degrees in applied physics from California Institute of Technology, Pasadena, in 1993 and 1996, respectively.

In 1997, he was an Assistant Professor at the University of South Carolina, Columbia, where he is currently a Professor of electrical engineering–electrophysics. His research interests include nanophotonics and photonic crystal devices.

Dr. O'Brien received the Presidential Early Career Award for Scientists and Engineers in 1999. In 2000, he received the NSF Career Award. He is currently an Associate Editor of IEEE Transactions on Nanotechnology.